

Evaluation of Local Bending in Profile-Wall Polyethylene Pipes

Ashutosh S. Dhar¹ and Ian D. Moore, M.ASCE²

Abstract: Thermoplastic pipes with a wide variety of wall geometries have been developed to obtain higher stiffness with utilization of less pipe material. The geometries of these profiles induce local bending, which may influence their structural performance. The localized deformations are investigated here for a range of commonly used pipe profiles using three-dimensional finite-element analysis. The study revealed that local bending governs the wall strains in some profiles. Among the three profile types considered, the effect of local bending was the greatest in the lined corrugated profiles. Circumferential strain distributions in the boxed and tubular profiles were almost uniform along the pipe axis, though axial and radial stress and strain indicated that these profiles also experienced local bending. While finite-element analysis using an axisymmetric idealization of the profiles appeared successful in capturing most of the characteristics of the three-dimensional profile response, certain aspects for the helically wound boxed profile were not captured well using this approach.

DOI: 10.1061/(ASCE)0733-947X(2006)132:11(898)

CE Database subject headings: Pipes; Bending; Geometry; Viscoplasticity.

Introduction

Thermoplastic pipes with different wall geometries have been manufactured to achieve effective utilization of pipe materials. A wide variety of wall geometries have been developed by the pipe manufacturing industry over the last few decades. However, the shapes of these profiles have led to questions regarding their impact on pipe performance. Hashash (1991) observed liner buckling and circumferential cracking on the inner walls of a lined corrugated pipe under a high embankment (30.5 m) near Pittsburgh, Pennsylvania. The localized short-wave deformation and inner wall tearing were also observed in honey-combed (tubular profile) high-density polyethylene (HDPE) pipes under 12.2 m fill in Ohio (Hurd et al. 1997). A recent study on field performance of 45 HDPE culvert pipes at different sites in South Carolina has revealed circumferential cracks in 18% of the pipes, localized bulges in 20% of the pipes, and tears or punctures in 7% of the pipes (Gassman et al. 2005). This study warranted further investigation to sufficiently quantify the problems. Moore and Hu (1996) demonstrated earlier from axisymmetric finite-element analysis that localized bending on profile components can produce significant tension at the liner-corrugation junction in lined corrugated HDPE pipes. The circumferential cracking reported by Hashash (1991), Hurd et al. (1997), and Gassman et al. (2005)

suggests that high axial (longitudinal) tensile stresses develop in these profiles.

Moore and Hu (1996) used finite-element analysis to show that axial tensions arise in lined corrugated HDPE pipes as a result of local bending, a three-dimensional (3D) phenomenon that cannot be estimated using conventional 2D shell theory. However, Dhar et al. (2004) demonstrated that the overall pipe responses (deflections and strains on elements not undergoing local bending) can be predicted effectively using the conventional 2D plane strain idealization.

Dhar and Moore (2004) investigated the behavior of four different profile-wall pipes based on full-scale laboratory tests under axisymmetric loading (inducing uniform hoop compression). Local bending is investigated here for each of those four profile-wall pipes, with the objective of developing a better understanding of the localized distress encountered in profile-wall pipes in the field. Comparisons of strain distributions for the four profiles are made to explore the effects of the profile shape on bending.

First, strain distributions in the walls of the pipes are evaluated using axisymmetric finite-element analysis for comparison with strain measurements obtained from the laboratory tests. The analysis is then extended to investigate pipe responses in a more realistic, biaxial stress field (biaxial stresses develop in the field, because horizontal earth pressures are generally less than vertical earth pressures). The 3D analysis includes explicit modeling of the profile geometries recorded from various test specimens (Dhar 2002).

Description of Profiles and Full-Scale Tests

Dhar and Moore (2004) investigated the performance of four different profile-wall pipes in biaxial and/or axisymmetric loading environments using full-scale tests. Two of the pipes investigated were lined corrugated (also known as “twin-wall”) profiles, one was a boxed profile, and the other was a tubular (also called “honey-combed”) profile. Fig. 1 shows the pipes and profile cross

¹Assistant Professor, Dept. of Civil Engineering, Bangladesh Univ. of Engineering Technology, Dhaka-1000, Bangladesh (corresponding author). E-mail: ashutoshdhar@ce.buet.ac.bd

²Professor and Canada Research Chair, GeoEngineering Centre at Queen's-RMC, Queen's Univ., Kingston ON, Canada. E-mail: moore@civil.queensu.ca

Note. Discussion open until April 1, 2007. Separate discussions must be submitted for individual papers. To extend the closing date by one month, a written request must be filed with the ASCE Managing Editor. The manuscript for this paper was submitted for review and possible publication on January 25, 2005; approved on March 24, 2006. This paper is part of the *Journal of Transportation Engineering*, Vol. 132, No. 11, November 1, 2006. ©ASCE, ISSN 0733-947X/2006/11-898-906/\$25.00.

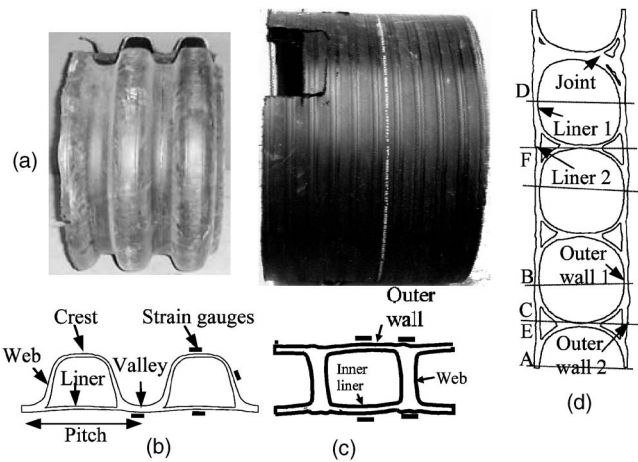


Fig. 1. High density polyethylene pipe profile: (a) pipes; (b) lined corrugated profile; (c) boxed profile; and (d) tubular profile

sections. One of the lined corrugated pipes had a corrugation spacing (pitch) of 80 mm and a corrugation depth of 58.7 mm; the other possessed a corrugation spacing of 101 mm and a corrugation depth of 55.2 mm. Thus, the spans of the liners were different in these two profiles. The components of each profile are defined in Fig. 1. The boxed profile pipe was manufactured by helical winding of the box section so that the central ribs were oriented at an angle of 2° to the pipe circumference. The tubular profile pipe was manufactured by spirally winding a unit of four tubes. The units were fused together at the ends. The helix angle for the tubular profile was approximately 6° from the pipe circumference. Nominal diameters for the boxed and tubular profiles were 760 and 1,060 mm, respectively.

In the axisymmetric loading test, the pipe was placed upright (vertical) concentrically within a steel cylindrical cell [the hoop cell; Moore et al. (1996)]. This test concept was originally proposed by Selig (Hashash 1991) and is an ideal means of investigating the local bending and buckling limit states associated with the profile geometry. The test evaluates the response of the pipe and the soil in its immediate vicinity to the uniform component of earth pressures $(\sigma_v + \sigma_h)/2$, the principal cause of local buckling and local bending in the profile. Experiments have been conducted placing the same pipe in the hoop compression cell and the biaxial pipe test cell (which more exactly models pipe burial conditions) (Dhar and Moore 2004). Those comparisons confirm that the hoop compression cell induces the same performance limits associated with local profile geometry, but with greatly reduced effort.

The pipe was backfilled using granular soil (an “SP” material, according to the Unified Soil Classification System). The backfill soil was placed in approximately 152-mm-thick layers, with each layer compacted using a tamper (4.5 kg mass). Height of fall of the tamper was approximately 305 mm to achieve a compaction of 80–90% of standard Proctor density, as established in various trials. Radial pressure was applied to the soil–pipe system using an inflatable air bladder lining the inner surface of the cylinder. The air pressure was measured using a pressure gauge and a conventional data acquisition system. The cell was axially restrained along with the pipe to attain a plane-strain condition, and the length of the tested pipe was the same as the length of the cell (1,450 mm). The diameter of the cell was 1,500 mm. Fig. 2 shows the arrangement of a pipe in the hoop cell during the test. Pipe deflections and strains on different pro-

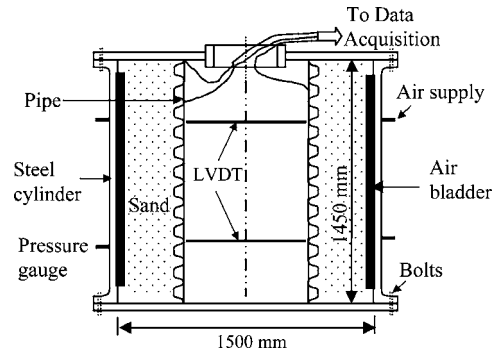


Fig. 2. Arrangement of pipe in hoop cell test

file elements were measured during the tests to capture the local bending. Normalized pipe deflections expressed as $\Delta D/D$ (for diameter D) equal the hoop strains, assuming that the soil density and stiffness is uniform around the pipe.

Finite-Element Model

Axisymmetric finite-element analysis was employed to investigate the response of the pipes under axisymmetric loads. Pipes with annular profiles have axisymmetric geometries; therefore, axisymmetric finite-element analysis with the finite-element mesh defined in the r – z plane can be used to define the problem geometry. Fig. 3 depicts typical finite-element meshes used for an annular pipe with a lined corrugated profile, boxed profile, and tubular profile (dimension L is defined as used later in the paper). The pipes are modeled as being very long, using smooth rigid (axially restrained) boundaries at the top and bottom of the mesh. The pipes were modeled in the analysis to simulate the test conditions in the hoop cell discussed earlier.

Fig. 3(a) shows the finite-element mesh used for analysis of the lined corrugated pipe in the axisymmetric loading test. The external diameter of the soil region around the pipe corresponds to the inner diameter, 1,500 mm, of the steel test cell. This provides a soil ring width of 430 mm surrounding the lined corrugated pipes. Finite-element meshes for the helically wound boxed and tubular profiles are shown in Figs. 3(b and c), respectively. Geometry of the pipe profiles was explicitly modeled in the analysis (Fig. 3). Though the geometry of the helical profiles is nonaxisymmetric, axisymmetric idealizations were used. This avoids the significant complexities of modeling the true spiral geometry. A comparison of calculated strains and those measured in the tests is used to investigate whether this axisymmetric approximation is reasonable for the helically profiled pipes. A soil ring of 335 mm width surrounded the pipe with a boxed profile. A 175 mm soil ring surrounded the pipe with a tubular profile.

Material Parameters

Pipe Parameters

Use of appropriate constitutive models is necessary to simulate reasonably the physical behavior using finite-element analyses. Thermoplastic material exhibits noticeable time-dependent behavior. However, elastic modeling using a secant modulus is the most widely used approach for thermoplastic pipe analysis because of its simplicity. Both a linear elastic model based on the secant

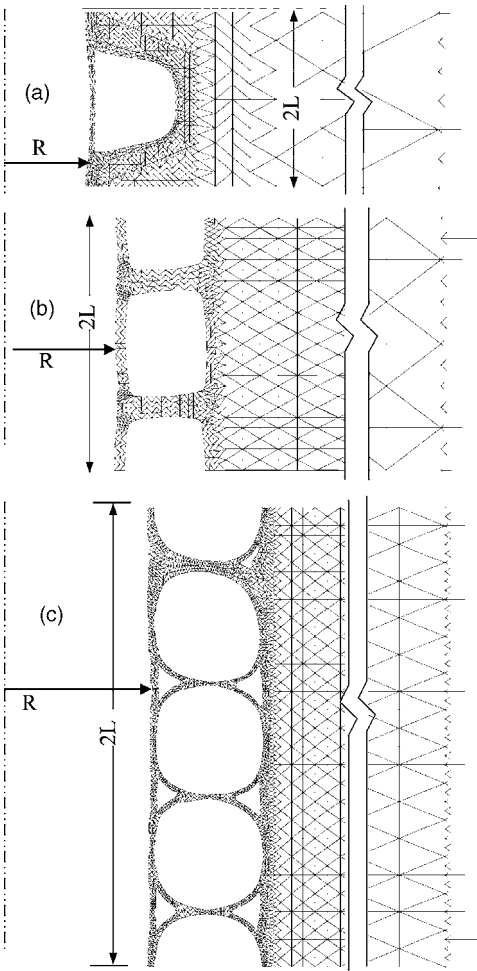


Fig. 3. Finite-element mesh for axisymmetric analysis: (a) lined corrugated pipe; (b) boxed profile pipe; and (c) tubular profile pipe

modulus at a particular elapsed time and the viscoplastic model of Zhang and Moore (1997) have been used in this study to analyze the pipes tested in the axisymmetric cell. Zhang and Moore (1997) developed a viscoplastic model for HDPE material after adapting the framework of Bodner's overstress theory (Bodner and Parton 1972). They determined two sets of viscoplastic model parameters for two HDPE pipe materials using uniaxial compression tests on cylindrical specimens (with 12.7 mm diameter and 25.4 mm height) cut from pipes obtained from the manufacturers of one of the lined corrugated pipes and the boxed profile pipe. Moore and Zhang (1998) successfully used the model for simulation of HDPE pipe response in a parallel plate test. These parameters are used in this study for simulation of pipe responses in axisymmetric tests. However, it is expected that the quality of the viscoplastic calculations for the profiles presented here could be

Table 1. Pipe Parameters Used in Finite-Element Analysis

Material model	E (MPa)	ν	C	n	γ (MPa)	$\beta \times 10^{-5}$ (MPa)	d_1 ($\times 10^{-3}$)	d_2	d_3 ($\times 10^{-2}$)
Linear model	450	0.46	—	—	—	—	—	—	—
VP model 1 ^a	1,350	0.46	0.01	8.0	10^{-4}	7.744	1.055	3.829	2.55
VP model 2 ^a	1,450	0.46	0.01	8.0	10^{-4}	7.056	1.042	3.829	2.55

Note: VP=viscoplastic.

^aZhang and Moore (1998).

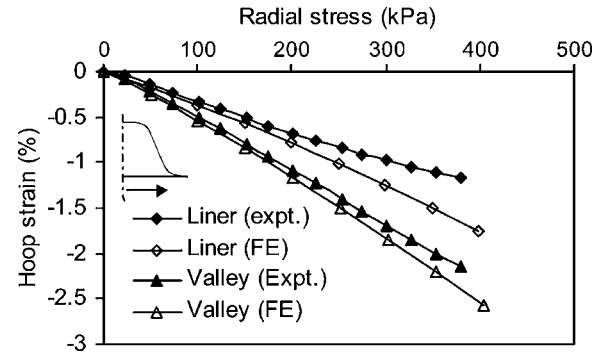


Fig. 4. Comparison of inner wall strains of lined corrugated profile

degraded somewhat because the specific material parameters for each of the test pipes were not available. Parameters used for the pipe materials are summarized in Table 1.

Soil Parameters

Stresses and deformations of the soil were not measured during the test in the hoop cell. The soil parameters used for the analysis were those reported by Zhang and Moore (1998), who undertook an analysis of a pipe tested in the same backfill. However, the degree of compaction achieved in each hoop compression test was variable, because compaction was difficult to control in the narrow space between the pipe and the test cell wall (Dhar and Moore 2004), even though an effort was made to achieve a compaction of the backfill as with those of Zhang and Moore (1998). Zhang and Moore (1998) used a modulus of elasticity, E , and Poisson's ratio, ν , for the soil of 30 MPa and 0.2, respectively.

An elastoplastic soil model based on the Mohr–Coulomb failure criterion was used in the analysis to capture shear failure during the pipe tests. For the elastic–plastic analysis, an angle of internal friction for the soil of $\phi=36^\circ$ was selected based on data suggested for material classified as “SW85” by Selig (1990). Angle of dilation was set as equal to the angle of internal friction (i.e., 36°), though one analysis was performed using a smaller dilation angle [i.e., 13° , a typical value for granular material; Skempton (1984)], which showed no significant change in the calculated pipe response (less than 1% deviation in calculated deformation).

Comparison of Wall Strains with Measurements

Lined Corrugated Pipes

Fig. 4 shows a comparison of the inner wall strains of a lined corrugated profile. Calculated strains generally provide a reasonable match with the measurements in Fig. 4, except at high radial

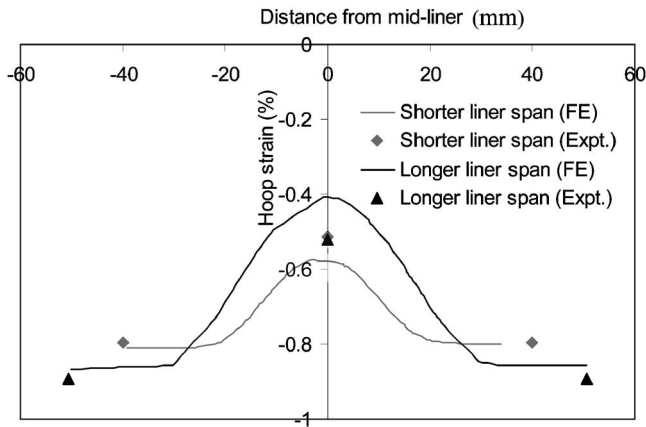


Fig. 5. Distribution of hoop strain on inner wall (at 150 kPa of radial pressure)

stress, when local buckling caused the liner strain to be stabilized (Dhar et al. 2004). Other comparisons were similar, but these are omitted for the sake of brevity. In Fig. 4, calculated circumferential strains on the liner are less than those on the valley, as recorded during the test. Distributions of calculated and measured strains along the interior surface of the two lined corrugated profiles are plotted in Figs. 5 and 6 at a radial cell pressure of 150 kPa, where the two figures show hoop and axial strains, respectively. It is evident from the figures that the hoop strains are not uniform along the inner surface of the lined corrugated profiles (even though the distance of the inner wall from the neutral axis of the profile is almost constant). Local bending of the liner has resulted in the compressive hoop strain varying from a maximum at the valley to a minimum at the midposition, where the liner spans between the valleys (Fig. 5). The mechanism of the bending can be explained using the deflected shape of the profile under load (Fig. 7). Solid lines in the figure represent the original position, and dotted lines show the deflected geometry. Local bending develops in the liner because it is forced to deform inwards where it is connected at the valleys, and inward movements decrease towards the liner midpoint. The local bending produces peak longitudinal (axial) bending strains in the liner at liner-corrugation intersection and bending strains of the opposite sign at the midpoint.

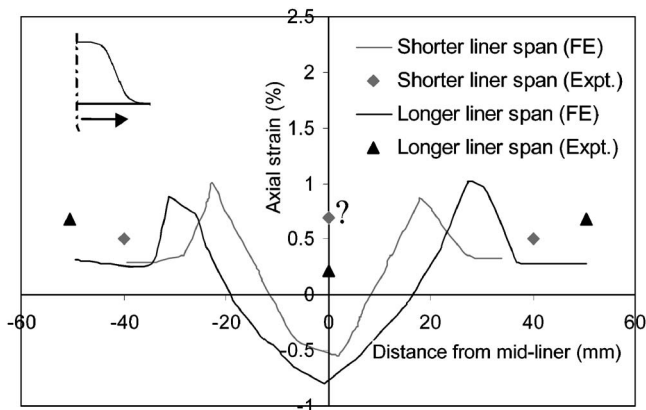


Fig. 6. Axial strain distribution in inner wall (at 150 kPa of radial pressure)

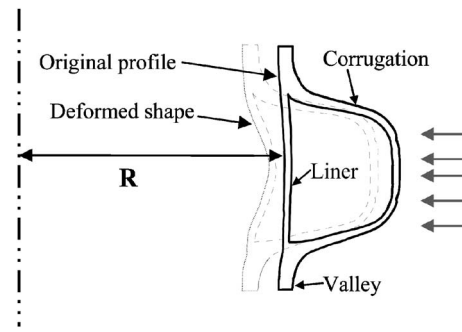


Fig. 7. Mechanism of local bending [after Dhar (2002)]

Analysis suggests that the circumferential liner strain is about 70% of the valley strain for the profile with a shorter liner span, while the measurement gave this percentage as 65%. The amount of liner to valley strain for the longer liner was 50%; the measured value was 60%. The magnitudes of the measured hoop strain at the midliner were somewhat lower than the calculated values, while calculated valley strains matched the measurements well. Further details of the analysis of the lined corrugated profiles are available elsewhere, (Dhar 2002).

The finite-element analysis indicates that there is a local increase in tensile axial strain at the liner-corrugation junctions of both profiles (Fig. 6). No measurements of strains were made directly at this position because of the difficulty of attaching gauges. Measurements of axial strain at other locations do not match those obtained from the analysis. The most likely explanation for this discrepancy is that changes in the local strain field occur where a strain gauge is adhered to the surface of a HDPE pipe (e.g., Brachman 1999). It appears likely that the effect of strain gauge “stiffening” is severe in regions of high strain gradients, particularly through the thickness of the liner element, so that axial strain measurements are poor (circumferential strains feature lower through-thickness gradients, so they are less affected by this phenomenon).

Boxed Profile Pipe

Fig. 8 presents axisymmetric finite-element calculations and measurements of pipe deflections for the helically wound boxed profile. In Fig. 8(a), the calculation using the viscoplastic HDPE model of Zhang and Moore (1998) better matches the measurements than calculations based on linear elastic material modeling and consequently only the results of the viscoplastic analyses are included in Figs. 8(b and c). The nonlinear time-dependent effects of the pipe material appear to noticeably influence the behavior. Use of viscoplastic material parameters that were established for a different HDPE pipe product may have contributed to the underestimation of the diameter decreases.

Hoop strains at the inner liner and outer walls of the boxed profile match the measurements well [Figs. 8(b and c)]. The hoop strain was measured as less than the deflection ratio (Δ/D) [Fig. 8(b)], though for axisymmetric behavior, the strain is expected to be the same as the deflection ratio. This discrepancy might have resulted because the profile has a helical geometry rather than the axisymmetric (annular) configuration modeled in the analysis.

The hoop strains under the web (on the interior surface) and over the web (on the exterior surface) were measured as much less than those on the liner (see Fig. 1 for definition of the profile

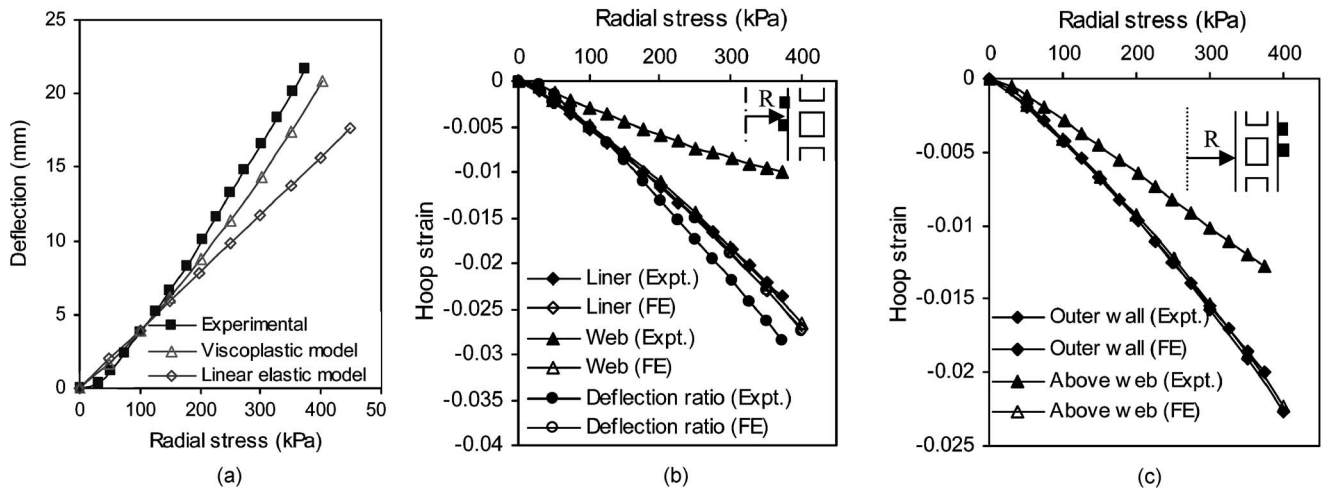


Fig. 8. Response of boxed profile pipe under hoop compression: (a) deflection; (b) hoop strains on interior walls; and (c) hoop strains on exterior walls

components). Measured strain under the web is about 50% of the liner strain on the interior surface [Fig. 8(b)], and the outer surface web strain is approximately 70% of the exterior surface value midway between webs [Fig. 8(c)]. The axisymmetric analysis produced almost the same values of strain on the web and liner. The helical winding of the rib may produce localized behavior within the profile which is not captured effectively using the axisymmetric idealization. The lateral element (the web) of the profile is very thick and when analyzed as axisymmetric will have a high hoop and torsional stiffness. In particular, a rib of helical geometry is likely much easier to twist under torsion, and this may have led to the lower hoop strains at the location of the rib.

It appears that there are limitations associated with the use of an axisymmetric idealization of the profile for calculation of local bending effects (wall strains) in the boxed profile. However, the diameter decrease was successfully estimated using the axisymmetric analysis, indicating that global response is not affected by the axisymmetric idealization. The axisymmetric analysis pro-

vided upper bounds for the hoop strains in the profile, so use in pipe design should produce conservative estimates of hoop stress and hoop strain.

Tubular (Honey-Combed) Profile

Fig. 9 shows calculated and measured values of diameter decrease and inner wall strains for a pipe with a honey-combed (tubular) profile. The axisymmetric finite-element procedure appears successful in estimating the pipe deflections for the profile. The viscoplastic model captured effectively the nonlinear nature of the pipe deflections in Fig. 9(a). Results of the viscoplastic analysis only are included in Figs. 9(b and c).

Strains on the tubular profile were measured on the inner liners and the outer walls of all the tubes of the unit [locations A, B, C, D, E, and F as shown in Fig. 1(c)]. This pipe was manufactured by helical winding of a unit of four tubes. Strain estimates at each of these locations show general agreement with the measurements [Figs. 9(b and c)]. With the exception of point B, which appears

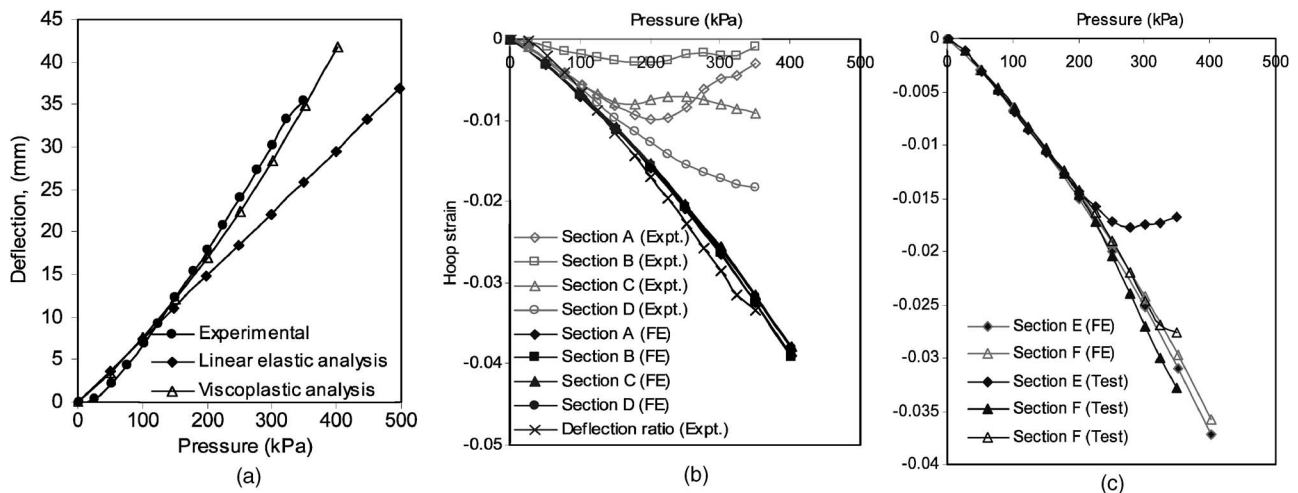


Fig. 9. Responses of tubular profile pipe: (a) deflection; (b) hoop strain on liner 1; and (c) hoop strain on liner 2

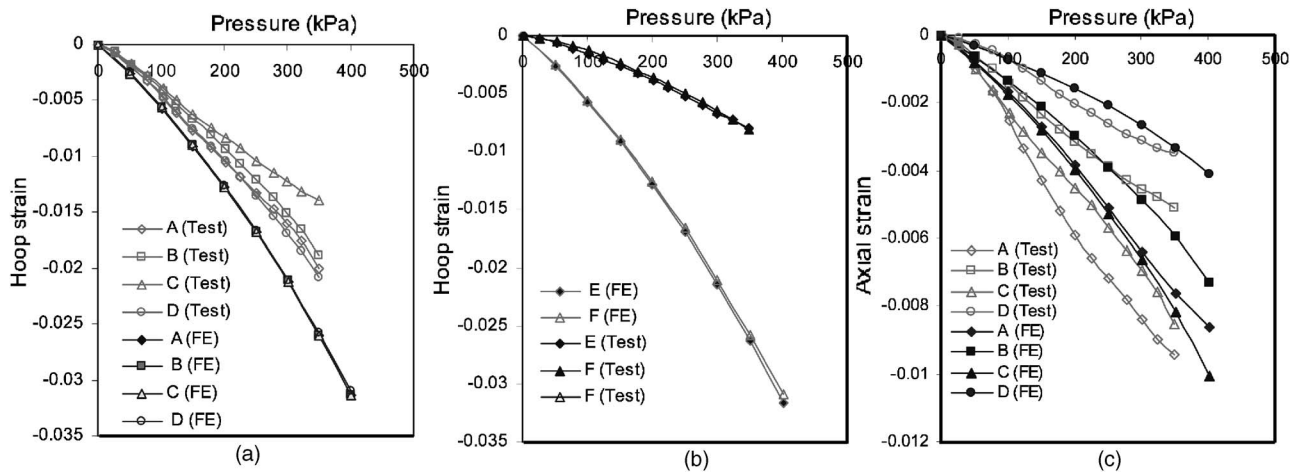


Fig. 10. Outer wall strains on tubular profile pipe: (a) hoop strains on outer wall 1; (b) hoop strains on outer wall 2; (c) axial strain on wall 1

to suffer from a gauging problem, hoop strains at the locations of the interior elements [the locations denoted as “liner 1” and “liner 2” in Fig. 1(c)] matched well, except at high load levels where certain elements showed the nonlinearity associated with local buckling [Figs. 9(b and c)]. The geometrically linear finite-element model could not capture the buckling, which is a geometrically nonlinear phenomenon. Geometry of the tubular profile was irregular, which affected significantly the local strains and the development of buckling. Fig. 10 shows comparisons of strains on the outer wall of the tubular profile. Hoop strains measured on outer wall 2 did not match the calculated values very well [Fig. 10(b)], whereas calculation of the strains on outer wall 1 performed better [Fig. 10(a)]. In both cases, measured strain was less than the calculated value. In particular, the section connecting the two tubes [the part denoted as “outer wall 2” in Fig. 1(c), the outer segment of the “tubes”] provided greatly reduced hoop strain measurements. This may have resulted from difficulties associated with making the local strain measurements on the outer surface, which is in direct contact with the surrounding soil, though in each case there were repeated measurements that provided similar low values. Axisymmetric idealization of the helical profile may also have caused the high strain calculation on the elements, as observed for the boxed profile discussed earlier.

Fig. 10(c) shows axial strain on outer wall 1 of this profile. Both calculations and measurements indicate that the axial strains at different locations of the profile are inconsistent, clearly the result of local bending associated with the irregular geometry. However, the comparison reveals that the helically wound tubular profile could be modeled more effectively than the boxed profile using an axisymmetric (annular) idealization. Perhaps this is because the walls are very thin for the tubular profile, so they provide little torsional rigidity.

Comparison of Local Strains in Different Profiles

Axisymmetric Compression

The study presented here reveals that finite-element analyses with explicit modeling of the profiles can be used to study various aspects of the 3D response of profiled pipes. An investigation of the 3D behavior of four pipe profiles has been included in this

section to compare the performance of different profiles. The 3D profile behavior under uniform radial compression is examined using axisymmetric finite-element analysis. Wall strains on different profiles have been examined for this comparison of profile performance.

Distributions of hoop strains on the inner surface of the four profiles at a radial cell pressure of 150 kPa are plotted in Fig. 11. Strains are normalized with the deflection ratio so that results for each pipe can be compared (because deformations are not the same on all pipes at a given radial pressure). Strain location is defined using z (the axial distance from the middle of the pipe longitudinal segment considered) normalized relative to L (half the axial length of the meshes shown in Fig. 3).

Fig. 11 shows that the boxed profile has circumferential strains at the surface of the inner wall that are calculated to be almost uniform. The strains for the tubular profile are less uniform. However, the hoop strains are not uniform along the inner surface of the two lined corrugated profiles. In the lined corrugated pipes, the strain at the center of the liner is a fraction of the valley strain due to the local bending. Between the two lined corrugated profiles, the one with a shorter pitch experiences larger com-

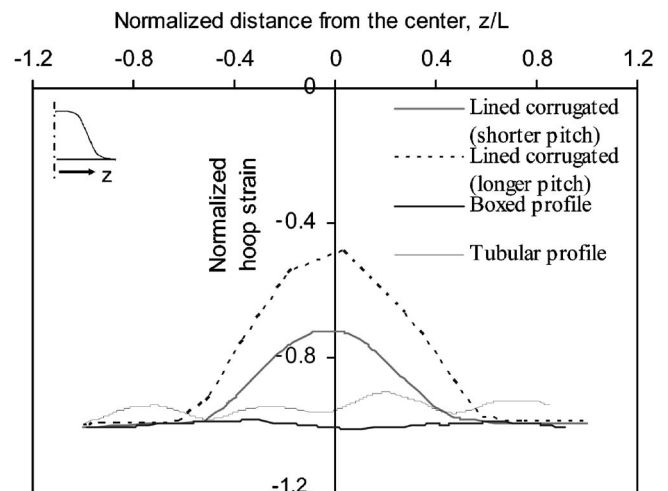


Fig. 11. Comparison of inner wall hoop strains in different profiles (at 150 kPa)

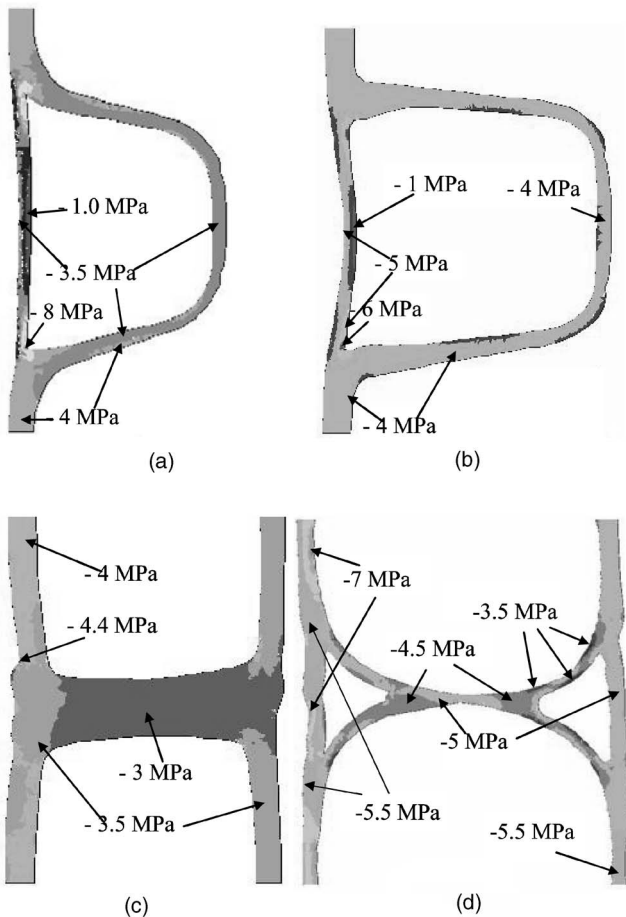


Fig. 12. Contour of circumferential stresses in each of the profiles: (a) lined corrugated profile with longer liner; (b) lined corrugated profile with shorter liner; (c) boxed profile; and (d) tubular profile

pressive hoop strain in the liner than the profile with a longer pitch. Strain at the middle of the liner is about 70% of the valley strain for the pipe with the shorter liner, whereas the liner mid-point has about 50% of the valley strain for the profile with the longer liner. Clearly, the span of the liner has a significant effect on the strains that develop in it. Not surprisingly, local bending within the liner leads to greater reductions in hoop strain when liner “span” (the distance the liner stretches between corrugation valleys) is increased.

Fig. 12 shows the contours of the hoop stresses in each of the profiles, plotted at the same radial pressure of 150 kPa. Compressive stress is denoted as negative in the figures. Fig. 12 reveals that a concentration of stresses develops at the liner–corrugation intersection in the lined corrugated profiles. Hoop stresses on corrugations in both profiles are approximately the same (–4 MPa), whereas the hoop compression at the intersection is twice that of the valley stress (–8 MPa) in the profile with the longer liner. The stress at the intersection for the other pipe is 1.5 times the valley stress. The maximum hoop stress on the boxed profile is located where the inner liner is connected to the rib [Fig. 12(c)]. Only a representative portion of the boxed and the tubular profiles is shown in Fig. 12. The maximum stress is somewhat higher than the liner hoop stress (the liner stress is –4 MPa and the maximum stress is –4.4 MPa), with no significant stress concentration in the boxed profile. The hoop stress in the tubular profile reaches a maximum (–7 MPa) at the

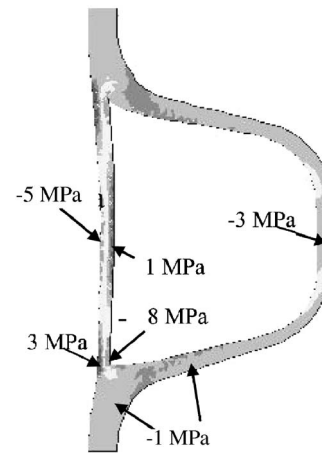


Fig. 13. Contour of axial stresses in lined corrugated profile

middle of both inner liners [Fig. 12(d)], while the average hoop stress within the profile is –5 MPa. This indicates that some local bending occurs in the profile with the tubular profile, because the diameter is larger.

Fig. 13 plots the contour of axial stresses in a lined corrugated profile (profile with a longer liner). Axial compression at the liner–corrugation connection is of similar magnitude to the hoop compression (–8 MPa; Fig. 12), even though axial stress in the valley itself is one quarter (–1 MPa) of that calculated in the hoop direction. Axial stress contours for the other profiles are not included here due to space restrictions. Fig. 13 again illustrates how axial tension develops on the outer surface of the liner–corrugation junction. The magnitude of the tension is half of the maximum compression on the inner surface (4 MPa). Thus, the circumferential compression and axial tension at the junction are the maximum distress the lined corrugated profile undergoes, and both should be considered when evaluating the performance of the lined corrugated profiles.

Biaxial Loading

The maximum stresses on each of the four profiles have been examined under more realistic biaxial earth pressures expected in the field. A semianalytical finite-element method (Moore 1995) was used to model the pipe in the biaxial stress field. The semi-analytical method employs a 2D finite-element mesh to model the pipe and the surrounding soil in the r, z plane (similar to those shown in Fig. 3), and a Fourier series is used to represent the variations around the pipe circumference. Pipes at two different depths of burial (2 and 8 m) have been examined for the short-term and long-term profile stresses in the circumferential, axial, and radial directions. Table 2 shows details of the

Table 2. Parameters for Semianalytical Finite-Element Analysis

Depth (m)	σ_v (kPa)	σ_h (kPa)	Soil (SW95) parameters		HDPE modulus (MPa)	
			ν	$M_s (E)$ (MPa)	Short-term	Long-term
2	40	13.3	0.2	18.3 (15.25)	700	150
8	160	53.3	0.2	24.6 (20.5)	700	150

Note: HDPE=high-density polyethylene.

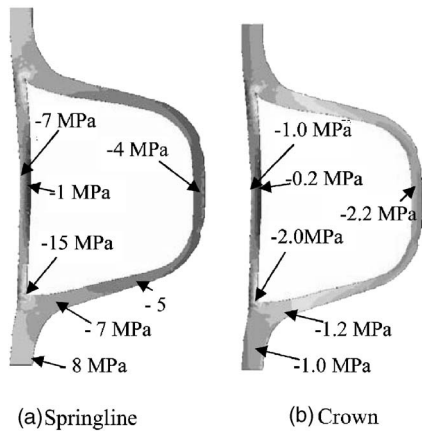


Fig. 14. Circumferential stress contours under biaxial loading (8 m burial)

parameters considered for short-term and long-term simulation. Well-graded sand compacted to 95% of the maximum Proctor density (SW95) has been considered as the backfill material. Parameters for the backfill soil at the stress levels corresponding to these depths (2 and 8 m) are estimated from McGrath et al. (1999).

Contours of the circumferential stresses at the springline and crown of a biaxially loaded lined corrugated pipe (profile with a longer liner span) buried at a depth of 8 m are plotted in Fig. 14. Nonuniformity of the stresses is evident in Fig. 14, which is similar to that seen under axisymmetric loading (Fig. 12). Fig. 14 reveals that maximum stress develops at the springline of the pipe for this profile. The locations of maximum stresses (within the profile) are the same as those observed under axisymmetric compression. At the crown, circumferential stresses on the outer surface of the pipe wall are greater than those on the inner surface due to increased radius of curvature (outward compression).

Springline stresses were the maximum for each of the profiles considered in this study. The locations of maximum stress were also the same as those for corresponding axisymmetric loading (shown in Fig. 12). Stress contours for the other profiles are not included here. However, the largest and smallest values of stresses in each profile are shown in Tables 3 and 4. Springline stresses only are included in the tables because they are the greatest for a biaxially loaded pipe. Tables 3 and 4 show the short-term and long-term stresses, respectively, at two different burial depths

Table 3. Maximum and Minimum Short-Term Stress at Springline

Pipe	Stress	Circumferential, σ_θ (MPa)		Axial, σ_a (MPa)		Radial, σ_r (MPa)	
		2 m	8 m	2 m	8 m	2 m	8 m
Twin-wall (longer liner)	Max	-4.2	-15.0	-4.0	-14.0	-1.6	-6.0
	Min	-0.4	-1.0	1.5	6.0	0.6	2.0
Twin-wall (shorter liner)	Max	-3.2	-11.5	-3.0	-11.0	-1.0	-3.4
	Min	-0.6	-2.5	1.4	5.0	0.2	0.6
Boxed	Max	-2.1	-7.8	-1.6	-5.5	-0.45	-1.6
	Min	-0.8	-3.2	0	0	0.15	0.6
Tubular	Max	-1.2	-4.2	-1.0	-3.4	-0.55	-1.8
	Min	-0.3	-1.2	0.1	0.6	0.15	0.4

Table 4. Maximum and Minimum Long-Term Stress at Springline

Pipe	Stress	Circumferential, σ_θ (MPa)		Axial, σ_a (MPa)		Radial, σ_r (MPa)	
		2 m	8 m	2 m	8 m	2 m	8 m
Twin-wall (longer liner)	Max	-1.9	-6.0	-1.8	-5.5	-0.7	-2.4
	Min	-0.2	-0.5	0.8	2.5	0.2	0.8
Twin-wall (shorter liner)	Max	-1.5	-4.8	-1.4	-4.5	-0.45	-1.4
	Min	-0.3	-1.0	0.6	2.0	0.05	0.2
Boxed	Max	-1.05	-3.6	-0.8	-2.6	-0.18	-0.60
	Min	-1.0	-1.8	0	0	0.08	0.30
Tubular	Max	-0.56	-1.8	-0.45	-1.8	-0.26	-0.90
	Min	-0.22	-0.8	0.05	0.2	0.06	0.20

(2 and 8 m). Long-term stresses are naturally less than short-term stresses due to the decrease in pipe modulus, which leads to additional positive arching. For each of the pipes and each burial depth, the long-term stresses are calculated to be about 40–50% of the short-term values.

The comparisons of maximum and minimum stresses in Tables 3 and 4 reveal that the greatest stress concentration occurs at the liner–corrugation junction of the lined corrugated pipe. The maximum short-term circumferential stresses at 8 m burial are -15 and -11.5 MPa, respectively, for the twin-wall pipes with a longer and shorter liner. The stresses on the boxed and tubular profiles at the same burial depth were -7.8 and -4.2 MPa, respectively. Using the American Association of State Highway and Transportation Officials (AASHTO) short-term stress limit of HDPE material (i.e., 20.7 MPa), it appears that local short-term stresses on the profiles are less than the short-term allowable stress. However, long-term stress on the twin-wall profile with a longer liner (i.e., 6 MPa) almost reaches the AASHTO long-term stress limit (i.e., 6.2 MPa), indicating that the long-term stress governs the design of this pipe.

Axial tension is also highest in the lined corrugated profiles. The boxed profile and the tubular profile showed smaller values of tension in the axial direction. However, axial tensile strain was measured on the boxed profile (Dhar and Moore 2004), which could not be captured using the axisymmetric idealization of this helically wound profile. Maximum compressive radial stresses for all profiles were smaller than the circumferential and axial values. However, the highest tensions in the boxed and tubular profiles appeared to develop in the radial direction.

The comparison reveals that the effect of local bending is particularly significant in the lined corrugated pipes. Local bending in the tubular and boxed profiles appeared less significant. Further work using full 3D finite-element analysis would be valuable to explore the effects of helical winding in more detail.

Conclusion

The 3D response of profiled pipes has been examined in this paper to develop an understanding of the 3D issues affecting the behavior of the profile geometries. The pipe profiles were modeled explicitly using geometries recorded from various test specimens. Results of the analysis were compared with measurements obtained using full-scale laboratory tests as reported by Dhar and Moore (2004). Three types of commonly used HDPE pipe profiles

(lined corrugated, boxed, and tubular) have been considered in the investigation.

The axisymmetric finite-element analysis was effectively used to model the response of the pipe profiles in an axisymmetric stress field. Modeling of the time-dependent nature of the polyethylene influenced the simulation of the laboratory hoop tests, and inclusion of these effects provided improved calculations. This is attributed to the fact that a relatively thin ring of soil is placed around the pipe in the hoop compression test cell, so the contribution of the pipe stiffness rather than the soil stiffness dominates the pipe behavior in this burial condition.

The axisymmetric assumption was less successful for the helically wound boxed profile, where it provided some values of hoop strain that exceeded measured values. The measurements of hoop strains on the walls were much lower than those obtained using the axisymmetric relation, Δ/D . However, calculations of pipe deflection (diameter change) were generally successful, indicating that global response is effectively calculated. Analysis of the helically wound tubular profile revealed that the finite-element analysis with axisymmetric idealization of the geometry provides a reasonable first approximation for the 3D profile response, though further work using 3D finite-element analysis would be valuable to explore the effects of helical geometry.

Local bending had a substantial effect on the stresses that developed in the lined corrugated profile. The effect was greater on the liner with a longer span. Strain distributions in the boxed and tubular profiles were almost uniform along the pipe axis, though axial stress values indicated that local bending also develops in those profiles. The locations of the maximum stresses were similar under both axisymmetric and biaxial loading for each profile, indicating that both hoop compression testing and axisymmetric finite-element analysis are useful means of understanding where zones of tension and compression develop in these structures.

Notation

The following symbols are used in this paper:

- $C, n, \gamma, \beta, d_1, d_2, d_3$
= viscoplastic parameters;
 c = cohesion;
 D = pipe diameter;
 E = modulus of elasticity;
 Δ = deflection;
 ν = Poisson's ratio;
 σ_h = horizontal earth pressure;
 σ_v = vertical earth pressure; and
 ϕ = angle of internal friction.

References

- Bodner, S. R., and Parton, Y. (1972). "A large deformation elastic-viscoplastic analysis of a thick-walled spherical shell." *J. Appl. Mech.*, 42(2), 385–389.
- Brachman, R. W. I. (1999). "Mechanical performance of landfill leachate collection pipes." Ph.D. thesis, Faculty of Engineering Science, Univ. of Western Ontario, London, Canada.
- Dhar, A. (2002). "Limit states of profiled thermoplastic pipes under deep burial." Ph.D. thesis, Dept. of Civil and Environmental Engineering, Univ. of Western Ontario, London, Canada.
- Dhar, A. S., and Moore, I. D. (2004). "Laboratory investigation of local bending in profiled thermoplastic pipes." *Adv. Struct. Eng.*, 7(3), 201–215.
- Dhar, A. S., Moore, I. D., and McGrath, T. J. (2004). "Two-dimensional analysis of thermoplastic culvert deformations and strains." *J. Geotech. Geoenviron. Eng.*, 130(2), 199–208.
- Gassman, S. L., Schroeder, A. J. A., and Ray, R. P. (2005). "Field performance of high density polyethylene culvert pipe." *J. Transp. Eng.*, 131(2), 160–167.
- Hashash, N. M. A. (1991). "Design and analysis of deeply buried polyethylene drainage pipes" Ph.D. thesis, Dept. of Civil Engineering, Univ. of Massachusetts, Amherst, Mass.
- Hurd, J. O., Sargand, S. M., and Masada, T. (1997). "Performance of large diameter HC-HDPE pipe under highway embankment in Ohio." *Proc., 76th Annual Meeting*, Transportation Research Board, Washington, D.C., Paper No. 970894.
- McGrath, T. J., Selig, E. T., Webb, M. C., and Zoladz, G. V. (1999). "Pipe interaction with the backfill envelope." *Publication No. FHWA-RD-98-191*, Federal Highway Administration, U.S. Dept. of Transportation, Washington, D.C.
- Moore, I. D. (1995). "Three-dimensional response of deeply buried profiled polyethylene pipe." *Transportation Research Record. 1514*, Transportation Research Board, Washington, D.C., 49–58.
- Moore, I. D., and Hu, F. (1996). "Linear viscoelastic modelling of profiled high density polyethylene pipe." *Can. J. Civ. Eng.*, 23, 395–407.
- Moore, I. D., Laidlaw, T. C., and Brachman, R. W. I. (1996). "Test cells for static pipe response under deep burial." *Proc., 49th Canadian Geotechnical Conf.*, Canadian Geotechnical Society, Alliston, Canada, 737–744.
- Moore, I. D., and Zhang, C. (1998). "Nonlinear predictions for HDPE pipe response under parallel plate loading." *J. Transp. Eng.*, 124(3), 286–292.
- Selig, E. T. (1990). "Soil properties for plastic pipe installations." *Buried plastic pipe technology*, ASTM, West Conshohocken, Pa., 141–158.
- Skempton, A. (1984). "Effective stress in soils, concrete, and rocks." *Selected papers on soil mechanics*, Telford, London, 4–16.
- Zhang, C., and Moore, I. D. (1997). "Nonlinear mechanical response of high density polyethylene. Part II: Uniaxial constitutive modeling." *Polym. Eng. Sci.*, 37(2), 414–420.
- Zhang, C., and Moore, I. D. (1998). "Nonlinear finite element analysis for thermoplastic pipes." *Transportation Research Record. 1624*, Transportation Research Board, Washington, D.C., 225–230.